

# High-performance tin-oxide supercapacitors using hydrazine functionalising assisted by hydrogen plasma treatment

Hassan Abdollahi<sup>1</sup>, Mahmoud Samkan<sup>1</sup>, Mohammad Ala Mohajerzadeh<sup>2,3</sup>, Zeinab Sanaee<sup>2,3</sup>, Shams Mohajerzadeh<sup>2</sup> ✉

<sup>1</sup>Department of Electrical Engineering, Shahid Sattari Aeronautical University of Science and Technology, Tehran, Iran

<sup>2</sup>Thin Film and Nanoelectronic Lab, School of Electrical and Computer Engineering, University of Tehran, Tehran, Iran

<sup>3</sup>Nano-fabricated Energy Devices Lab, School of Electrical and Computer Engineering, University of Tehran, Tehran, Iran

✉ E-mail: mohajer@ut.ac.ir

Published in Micro & Nano Letters; Received on 5th April 2019; Revised on 28th July 2019; Accepted on 15th August 2019

For the first time, the effects of adding hydrazine solution to tin-oxide sol-gel to be used as an electrode in high-performance supercapacitors have been studied. The mixed solution has been spin-coated on stainless steel foils as substrates followed by exposing to hydrogen plasma treatment. The results show the effectiveness of adding hydrazine to tin-oxide sol-gel, compared to pure tin-oxide sol-gel. The electrochemical tests such as cyclic-voltammetry and charge-discharge characteristics have been conducted, and the findings demonstrate the favourable contribution of adding hydrazine in increasing the capacitance of the supercapacitor. The physical properties of the tin-oxide material have been analysed by means of FESEM, XRD, TEM, FT-IR spectroscopy and Raman spectroscopy to have a better understanding of preparation procedure and better insight in material synthesis. The electrochemical tests demonstrate a high capacitance of 18 mF/cm<sup>2</sup> for the sample treated with hydrazine during the sol-gel processing which is around 40% higher than the merely prepared tin-oxide sample. The measured values for the capacitance versus rate show a rather linear correlation between these parameters, further corroborating an electric-double layer-based performance for such devices.

**1. Introduction:** Supercapacitors are among the most important energy-storing devices which possess higher power density compared to batteries owing to their rapid charge-discharge capability. The high charge-discharge rate originates from the evolution of an electric double layer or redox reactions at the surface and not within the bulk [1–4]. In general, supercapacitors are divided into two distinct groups; the first group of devices are governed by the so-called electrical-double layer capacitance (EDLC), while the second group of such energy-storing units are considered as pseudo-capacitance. Essentially, EDLC-based devices operate on reversible non-Faradic reactions (redox) which take place between the electrolyte and the electrode surface due to the accumulation of charged ionic species and they are mostly carbon-based materials. On the other hand, pseudo-capacitances are based on Faradic reactions which take place between interfaces. As a result, the double-layer devices last longer than pseudo-capacitances and possess higher power densities. However, they suffer from a lower capacitance energy density because only the surface is involved in energy-storing reactions [5–12].

Most of the materials which are being practiced for pseudo-capacitances are metal-oxides such as rare-earth elements like Ru or conductive polymers. While the former structures are expensive, the latter ones suffer from poor electrical conductivity. One of the great candidates for pseudo-capacitance is tin-oxide owing to its high capacitance and ability to be incorporated directly on stain-steel foils. This capability allows the formation of flexible capacitors where a role-to-role fabrication is also possible [13–15]. Tin oxide is a well-known material which has great applications in various fields such as gas sensor fabrication, catalysts, transparent conducting electrodes and finally, storing energy applications like anode electrodes for lithium-ion-battery or electrode for supercapacitance devices. The importance of this material in different applications has been a driving force to pave path for different fabrication methods. The sol-gel solution is found to be a favourite technique for the formation of highly porous structures, suitable for energy storing applications [16–19].

In this study, we have taken advantage of sol-gel solutions to establish a facile and inexpensive method to functionalise tin-oxide sol-gel with hydrazine solutions assisted by hydrogen plasma treatment. During plasma treatment, H-ions impinge the surface of the sample and help to reduce the Sn–O bonds, which in turn led to the formation of tin-rich nanostructures. In addition, the energy imparted from hydrogen ions to the lattice network of the substrate would help to rearrange the atoms and improve their chance of recrystallisation. The fabricated tin-oxide nanostructures have been used as electrodes for high-performance supercapacitors which have been realised directly on stainless steel foils. The significant effect of hydrazine functionalisation has been demonstrated using electrochemical tests of the final devices. Essentially hydrazine acts as a reducing agent to functionalise tin-oxide sol-gel and to convert tin oxide (or stannic oxide) phase into tin (II) oxide (stannous oxide) phase. To have a better insight into such synthesised materials, we have used various physical characterisation tools like SEM, TEM, Raman spectroscopy and XRD. Moreover, the results of electrochemical tests are reported to depict the deep effect of such functionalising treatment on the final performance of these energy storing devices.

**2. Experimental:** In this line of research, we have used stainless steel foils as substrates for the formation of supercapacitor devices. After initial cleaning in acetone, the stainless foils are first functionalised by means of HF/HNO<sub>3</sub>/water to induce the surface of the substrate with little pores and make the surface a little porous. The presence of hydrofluoric acid in this solution is critical to arriving at desired porosity and surface adhesion. Immediately after this cleaning step, we have coated the surface of the foils by tin oxide sol-gel solution, which is a mixture of SnCl<sub>4</sub> (as in source) and ethanol (as a solvent) with small amount of DI water. Once the solution is ready, we can add hydrazine to the sol-gel with a trace ratio of 1:15 (one hydrazine in 15 sol-gel). The prepared solution is then spin-coated on stainless substrates. Afterwards, the samples are placed in an oven to gradually raise the temperature to 200°C and to vaporise solvents

from the original solution. At this stage, the sample is also dried to become ready for the subsequent hydrogen plasma treatment which is being practiced in direct-current plasma reactor. After the samples are loaded in the dc-plasma reactor, the reactor chamber is evacuated by means of a rotary mechanical pump to reach a base pressure of 60 mTorr. After a short time, hydrogen gas flows into the reactor with a flow rate of 30 sccm to purge the chamber and prepare the reactor for the desired temperature to set. Under the flow of hydrogen gas and without plasma, the sample temperature rises to 300°C. Once the substrate temperature is set at its desired value, the proper electrical signals are applied on the electrodes to turn on the plasma and initiate the treatment. At this stage a plasma current of 50 mA with a voltage of 380 V is applied. During this plasma treatment, hydrogen ions bombard the surface of the sample for 10 min and finally, the plasma is turned off. The sample is let to cool down naturally while the hydrogen flow is maintained at its previous value. After the temperature is low enough, the hydrogen flow is terminated and after proper pumping down cycle, the reactor is vented and the sample is unloaded. The samples are now ready for further characterisation and CV measurements.

For physical characterisation of the prepared materials, we have extensively used Scanning Electron Microscopy (Hitachi S4160 FESEM), Transmission Electron Microscopy (Philips CM300, operating voltage at 200 kV), Raman spectroscopy (excitation wavelength of 532 nm, 10 mW power), Fourier transform infrared (FT-IR) and X-ray diffraction analysis. While the SEM measurements can be carried out on the stainless foils (although in some cases, a gold-coating might be needed), the TEM (HR-TEM) observation requires scratching the deposited tin-oxide film from the surface of the substrates, dissolving the powder in ethanol and drop-casting on standard TEM copper grids. Also for the FTIR analysis, we have to scratch the deposited tin-oxide film from the surface of the substrates and mix it with KBr powder. Raman spectroscopy and XRD analysis can be practiced directly on stainless foils without any further preparation. For electrochemical analysis, we have used a three-electrode setup, consisting of the platinum counter electrode, the Ag/AgCl reference electrode and the working (sample) one. All these three electrodes are in 1 M NaOH solution as an electrolyte.

Fig. 1 demonstrates the schematic diagram for the preparation and synthesis steps of these energy storing devices. First, the tin-oxide sol-gel solution mixed with hydrazine solution is shown. After proper agitation and mixing the solutions, spin coating of the final solution is performed on stainless substrates. The coated samples are then placed in the oven to dry out. To complete the functionalisation, the samples are placed in a hydrogen plasma reactor at an elevated temperature and under various

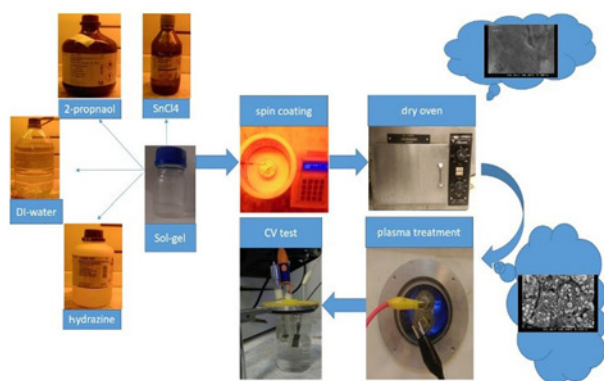


**Fig. 1** Brief schematic diagram of sample preparation for a supercapacitor test. The starting point is the formation of the sol-gel solution followed by spin coating on stainless foils. After the initial drying in a thermal oven the sample is exposed to hydrogen plasma to complete the fabrication procedure

plasma powers. Finally, the fabricated samples are subjected to electrochemical tests to correlate the results with the preparation conditions.

**3. Results and discussions:** Figs. 2 and 3 collect the results of SEM analyses on various samples prepared for this investigation. Figs. 2a and b show the images pertaining to two different samples which belong to mere sol-gel prepared sample (shown in Fig. 2a) and sol-gel/hydrazine solution sample (shown in Fig. 2b), respectively. Both samples have been prepared by spin-coating followed by pre-baking at 200°C for 15 min to remove solvents and just prior to a hydrogen plasma treatment. As seen from either image, the samples possess smooth and conformal surfaces and lack a porous structure. By referring to Fig. 2b, it is observed that the sample which has been exposed to hydrazine solution, the surface features are more pronounced compared to the mere sol-gel sample. Inset in Fig. 2b depicts a magnified image of the surface of the sample which demonstrates its porosity. In order to highlight the effect of plasma treatment on the morphology of the samples, we have conducted similar experiments except for the plasma treatment step. Figs. 2c and d show the evolution of textures on the surface of two samples made of hydrazine and sol-gel where the plasma treatment has been skipped for the first one (Fig. 2a). As seen, the surface texturing is more evident in the latter case where a plasma treatment has been practiced.

Figs. 3a and b display the SEM micrographs of the samples which have been prepared without and with a hydrazine solution during sol-gel processing and after being exposed to DC hydrogen plasma treatment at an elevated temperature of 300°C. As seen, the exposure to a hydrogen plasma treatment would lead to the formation of surface roughness and a highly textured structure is evolved. Fig. 3a corresponds to a mere tin-oxide sample, whereas Fig. 3b belongs to a hydrazine treated sample. All other specimen preparation steps remain identical for all samples. In general, by exposing the tin-oxide samples to hydrogen plasma, discernible

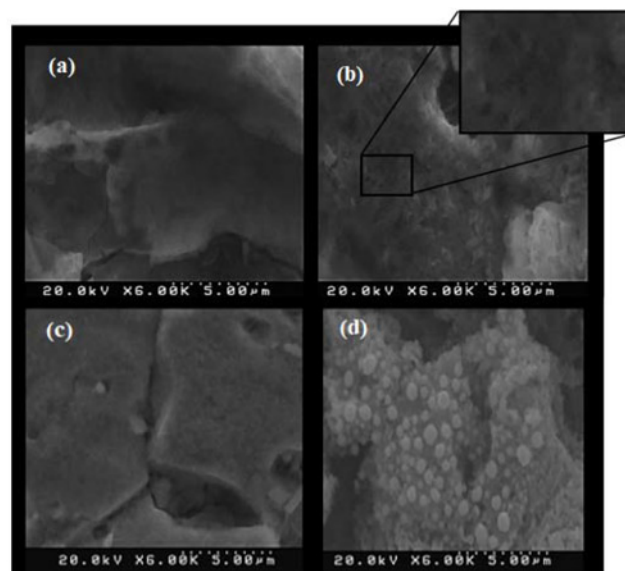


**Fig. 2** FESEM pictures of two different samples on stainless substrates after heating at 200°C in an oven to remove solvents just before DC plasma treatment

a Image of the sample prepared using pure tin-oxide sol-gel and b Sample obtained by mixing tin-oxide sol-gel with diluted hydrazine solution. The inset of Fig. 2b clearly shows the presence of little holes and pores in the sample. (c) and (d) Effect of plasma treatment on the surface morphology of the samples  
c Without plasma treatment and d With a plasma treatment step

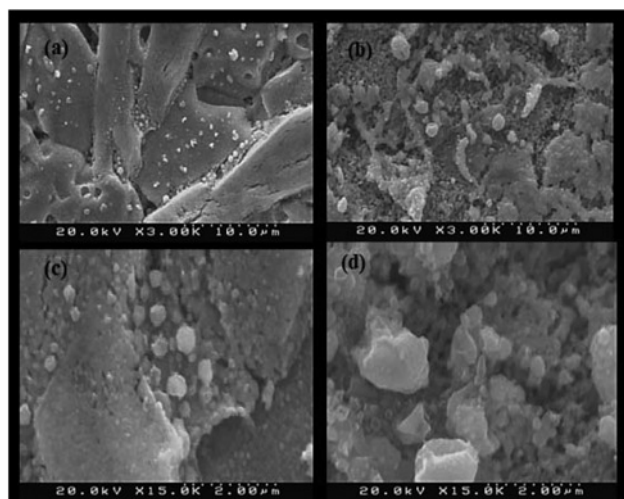


**Fig. 3** FESEM images of two different samples on a stainless substrate after similar hydrogen direct-current plasma treatment at 300°C  
*a* Sample made of pure tin-oxide sol-gel and  
*b* Sample of hydrazine-treated tin-oxide sol-gel solutions  
*c* and *d* Higher magnification images of these samples to show the evolution of bright spheres which is conceived to be tin-rich or tin islands

surface features are evolved, although this surface featuring is more pronounced for the hydrazine treated one (Fig. 3*b*). Such surface features are favourable for electric double layer enhancement of such capacitors due to an increased effective surface and to add up to the pseudo-capacitance nature of tin-oxide. Comparing these samples, it is deduced that a combined process of hydrazine functionalising and hydrogen plasma treatment would lead to a significant increase in the porosity and surface features of tin-oxide layers on stainless foils.

We believe that apart from surface features, hydrazine helps to convert tin-oxide into tin-rich islands. From the SEM images, some bright spheres can be observed which are assumed to be tin-rich (or tin) islands which form during the hydrogen plasma treatment step. The functionalising pre-treatment expedites this island formation and smaller and more sparsely distributed features are evolving. These spheres are important species to improve the conductivity of the layer and it is useful for electrochemical tests. Although not clearly observed by SEM, the nature of these spheres seems to be a core-shell structure as observed by a TEM apparatus as collected in Fig. 4.

Fig. 4 collects some of the TEM images of various samples prepared for this investigation. The results of this analysis correspond to the SEM images in Figs. 2 and 3. From these observations, it can be seen that the samples prepared with dilute hydrazine solution possess a more conformal and homogeneous structure with a rather regular shape, while the sample prepared with pure tin-oxide sol-gel, the structure is more granular and non-uniform. It is speculated that the addition of hydrazine during sol-gel treatment would induce sites for crystallisation which leads to higher regularity and better crystallinity. Figs. 4*c* and *d* present another location of similar samples further confirming the uniformity of the structuring for hydrazine-treated samples. Finally, Figs. 4*e* and *f* demonstrate the electron diffraction pattern to corroborate the higher degree of crystallinity of the hydrazine-treated samples. As seen, the diffraction patterns of both samples show rings indicating a poly-crystalline nature of the grains. However, the sharpness of the rings, which is an indication of the degree of crystallinity, is more pronounced for the hydrazine-treated specimen. Similar to Figs. 4*a* and *b*, Figs. 4*c* and *d* show regular shapes. It is also observed that for the hydrazine-treated samples, a core-shell structure is evolved, as shown by an arrow. Finally, to better observe the critical effect of plasma treatment on the crystallinity of the samples, we have

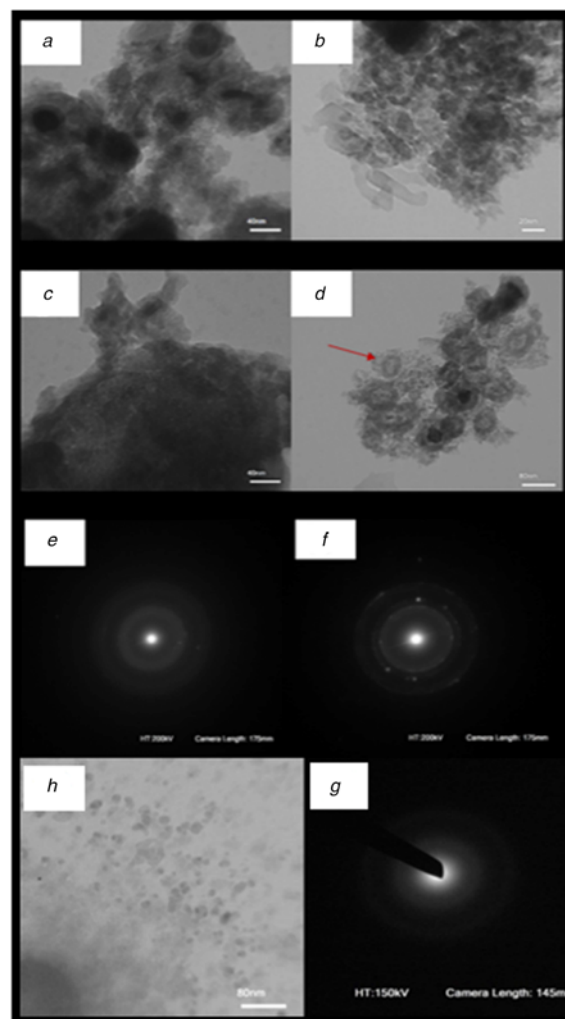


**Fig. 4** TEM image of similar samples prepared without and with hydrazine solution during sol-gel formation  
*a, c* While the left images correspond to mere sol-gel solution  
*b, d* Right-side images belong to the samples prepared using a hydrazine solution. Both the grain formation and crystallisation are more obvious for the samples which have been treated with hydrazine. A core-shell structure is observed for hydrazine-treated samples  
*e, f* Electron diffraction patterns support the crystallinity of the film and corroborate the effect of hydrazine in texturing and crystallisation of the samples  
*g* Bright-field TEM image of a processed sol-gel coating prior to plasma treatment and  
*h* Its corresponding electron diffraction pattern showing an amorphous structure

provided the bright field image (Fig. 4*g*) and diffraction pattern (Fig. 4*h*) of a tin-oxide prior to hydrogen plasma treatment. The amorphous nature of the layer is quite evident from the observed diffraction pattern in Fig. 4*h* of this figure.

In Fig. 5, we have collected the results of XRD analysis on different samples prepared for this study. The samples are similar to the ones previously observed with SEM and TEM characterisations. Fig. 5*a* belongs to mere tin-oxide sample, whereas Fig. 5*b* corresponds to the spectrum of the hydrazine-treated sample. Both of these samples have experienced a plasma treatment after drying in an oven at 200°C. There are three strong peaks correlated with the stainless substrate, which are identified by red arrows. More importantly, the SnO<sub>2</sub> and SnO peaks are represented by blue and green arrows, respectively.

Both of these samples show the main peak of rutile tin-oxide (SnO<sub>2</sub>) located at about 35°, although sample 'b' had stronger



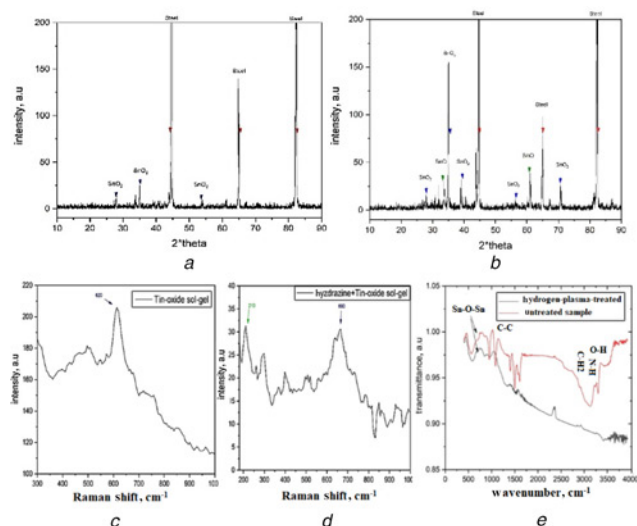


**Fig. 5** XRD analysis of various samples prepared for this investigation  
*a, b* Sample 'a' is a pure tin-oxide and sample 'b' corresponds to a mixture of hydrazine and tin-oxide sol-gel. The crystalline peaks corresponding to  $\text{SnO}_2$  constituent are more pronounced in the sample prepared with hydrazine  
*c, d* Corresponding spectra from Raman spectroscopy further confirming the improved crystallinity of the hydrazine-prepared samples  
*e* FT-IR spectroscopy of two samples which have been prepared with hydrazine-sol-gel but treated and untreated with hydrogen plasma. The peaks due to Sn-O bonds become smaller for the plasma-treated sample indicating a reduction to tin-rich structures

peak than 'a' which is due to the presence of hydrazine in the tin-oxide sol-gel that helps in crystallising of the tin-oxide layer. The presence of an intermediate phase of SnO peaks in sample 'b' is more evident owing to the fact that hydrazine acts as a reducing agent in the sol-gel solution to alleviate the formation of  $\text{SnO}$  phases. From the XRD analyses one can conclude that the hydrazine-treated tin-oxide material contains both phases of SnO and  $\text{SnO}_2$  at the same time [16–22]. The formation of SnO seems to be more favourable for the final energy storing devices. Figs. 5c and d depict the Raman spectra of two tin-oxide samples which have been prepared without and with a hydrazine treatment. Both of these samples have gone through the same hydrogen plasma conditions at 300 °C. For the former sample (Fig. 5c), the main peak is located at about 620  $\text{cm}^{-1}$  (marked by the blue arrow), which corresponds to the main Raman peak of  $\text{SnO}_2$ . From Fig. 5d, one can see that there are two obvious peaks at about 210  $\text{cm}^{-1}$  (marked by the green arrow) and 660  $\text{cm}^{-1}$  (marked by the blue arrow) related to main Raman peaks of SnO and  $\text{SnO}_2$  structures, respectively. The intensity of the peak at 210  $\text{cm}^{-1}$  Raman shift is comparable to the main  $\text{SnO}_2$  phonons at 660  $\text{cm}^{-1}$  wavenumber. We conclude that the sample prepared by a hydrazine-treatment comprises of two SnO and  $\text{SnO}_2$  phases (Fig. 5d). The Raman findings are in agreement with the XRD results where possess peaks attributed to SnO phase [23–27].

Although understanding the chemistry of the plasma treatment is a challenging matter, we have conducted FT-IR spectroscopy to examine different chemical bonds in the processed materials with and without a hydrogen plasma treatment. For this purpose, we have conducted FT-IR measurement on two samples which have been prepared with a mixture of hydrazine and tin-oxide sol-gel. One sample has been examined without hydrogen plasma-treatment while the other sample has been treated with a hydrogen-plasma. Other preparation steps have been identical for these samples. In Fig. 5e, the red plot represents the data from the untreated sample. As seen, there is a broad peak at about 3100  $\text{cm}^{-1}$  which is due to the N-H asymmetric stretching mode of hydrazine.

Also, peaks at about 3400, 1100 and 2900  $\text{cm}^{-1}$  are due to the O-H stretching mode, C-C and the  $\text{CH}_2$  bonds of isopropanol constituents in the sol-gel solution, respectively. All these peaks vanish or shrink with the help of hydrogen plasma at 300 °C. On the other hand, the peaks between 600 and 1000  $\text{cm}^{-1}$  wavenumber are related to Sn-O-Sn symmetric and anti-symmetric vibrations in the lattice structure. By comparing the results of the sample without plasma treatment with the plasma-treated sample, one can observe that the level of tin-oxygen peaks is reduced. This reduction is consistent with the observed images from SEM examinations where tin-rich spherical or ellipsoidal features are evolved. Plasma treatment with hydrogen would, in general, alters the tin-oxide into tin-rich nanostructures which form small islands and dots, and consequently increase the effective surface. This increase, in turn leads to an increased capacitance for the fabricated supercapacitors. Therefore, not only the surface texturing of the sample is improved during hydrogen-plasma treatment, tin-rich nanostructures are evolved which seem to be suitable for supercapacitance applications.

**4. Electrochemical tests:** In this section, we study electrochemical properties of samples at different scan rates of 10, 20, 50 and 100 mV/s in the range of –500 to 500 mV applied voltages. In addition, the charge-discharge test has been carried out at 0.5  $\text{mA}/\text{cm}^2$ . For such measurements, we have employed a three-electrode setup where one electrode acts as a counter (Pt), one as a reference (Ag/Ag/Cl) and the last one is the working electrode which contains the sample. A 1 M sodium hydroxide (NaOH) solution is also used as an electrolyte for this electrochemical analysis. Figs. 6a and b present the cyclic-voltammetry plots at four different scan rates (10, 20, 50 and 100 mV/s), where Fig. 6a relates to the hydrazine-treated sample (a mixture of tin-oxide, and hydrazine solutions) and Fig. 6b belongs to the pure tin-oxide sol-gel sample. As seen from both parts, all the measurement profiles behave similarly and without any discernible redox peak. The partially symmetric and parallelogram shape of these curves corroborate the assumption of a double-layer based performance. Since the cyclic-voltammetry

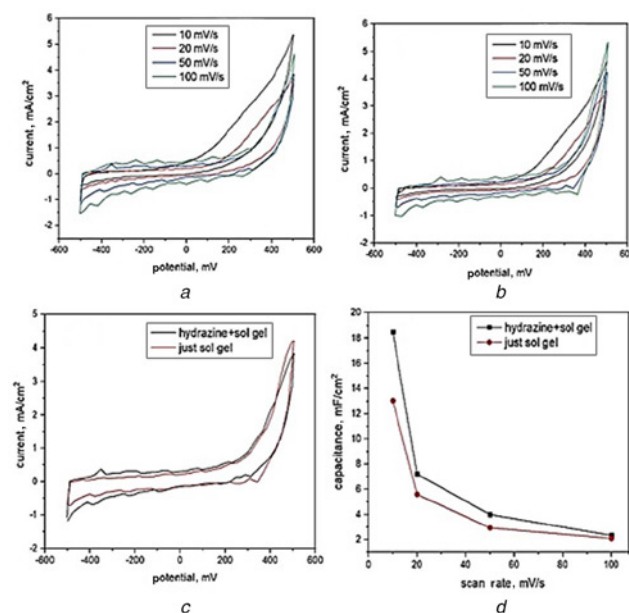


**Fig. 6** Cyclic voltammograms of  
*a* Sample with mixture of tin oxide sol-gel and hydrazine solutions at four different scan rates in the range of –500 to 500 mV  
*b* Sample with just tin-oxide sol-gel  
*c* CV plots of these samples at 50 mV/s scan rate  
*d* Capacitance versus scan rates plot of the prepared samples indicating a monotonic drop in the value of capacitance with respect to the scan rate

results for all the samples show a stretched parallelogram without any distinct peak, the supercapacitor behaviour for these nanostructures is believed to be mostly EDLC rather than pseudo-capacitor.

To have a better insight into the electrochemical behaviour of such supercapacitors, we have shown the cyclic-voltammetry experiments at a constant scan rate of 50 mV/s, as plotted in Fig. 6c. Once again, the general behaviour of both samples remains similar, but the hydrazine-treated sample illustrates a 30% improvement of the measured capacitance as opposed to pure tin-oxide sol-gel sample. Fig. 6d depicts the plot of capacitance versus scan rate for these samples to highlight the differences. At lower scan-rates, the capacitance of hydrazine-treated sample is far superior compared to the purely treated tin-oxide. This difference is >40% for the lower scan rate of 10 mV/s. To grasp an immediate insight into the obtained values for CV test, we have completed and collected the data in Table 1.

Finally, we have measured the stability of the capacitance by taking charge-discharge test of samples for 200 cycles at a current of 0.5 mA/cm<sup>2</sup>. At the first cycles (around 70 cycles) sample with hydrazine shows a larger capacitance than the

**Table 1** Extracted values for different scan rates of samples with pure tin-oxide sol-gel and tin-oxide sol-gel plus hydrazine solution

Material	Capacitance, mF/cm <sup>2</sup>			
	Scan rate			
	10 mV/s	20 mV/s	50 mV/s	100 mV/s
hydrazine-treated	18.54	7.22	4	2.34
tin-oxide sol-gel	13.05	5.6	2.94	2.1

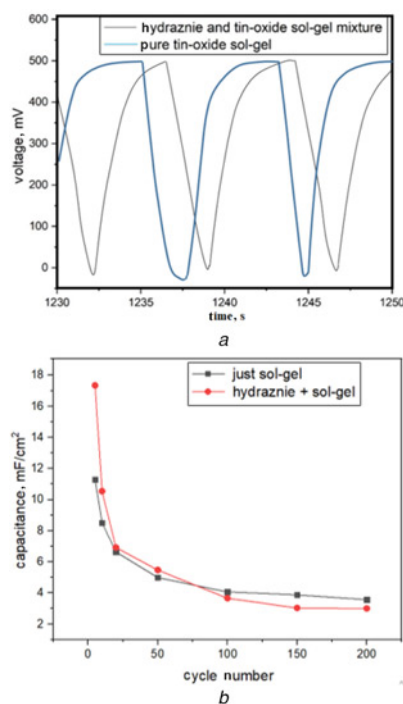


**Fig. 7** Galvanostatic measurements

a Charge-discharge versus time for two selected periods. Compared to the hydrazine-sol-gel prepared sample (grey curve) the pure sol-gel sample (blue curve) is faster indicating a smaller capacitance  
b Charge-discharge versus cycle number plot of samples with sol-gel/hydrazine and sol-gel prepared samples

sample of just pure sol-gel, hence the differences of capacitances value of at first cycle. At around 70th cycle the capacitances of both samples reached similar values, and further cycling does not show much difference in either electrode. The reason for this drop could be the dissolution of tin/tin-oxide core-shells which are more probable for the hydrazine-treated sample. This adverse effect is under investigation and needs to be alleviated before an industrial production is conceivable (see Fig. 7).

**5. Summary:** In summary, we have introduced an inexpensive and facile procedure by mixing hydrazine and tin-oxide sol-gel solutions in a diluted manner to functionalise the sol-gel prior to plasma treatment. Flexible stainless steel foils have been exploited as the substrates for the fabrication of high-performance supercapacitors. An extensive study of tin-oxide layers realised by means of hydrazine-treatment shows the evolution of bright spherical shapes in the form of yolk-shell configuration which is believed to be tin-rich islands. The electrochemical tests also demonstrate the beneficial effect of the hydrazine treatment to achieve higher values of capacitance superior to tin-oxide layers. A high value of 18 mF/cm<sup>2</sup> has been obtained at a scan rate of 10 mV/s which is 40% higher than the merely prepared sample. In addition, the behaviour is believed to be mostly dominated by the electric double layer and not by the Faradaic redox reactions. Despite the high performance of such devices, their stability is still a concern and further investigation of their long-term operation needs to be carried out.

## 6 References

- [1] Kuok F.H., Liao C.Y., Chen C.W., *ET AL.*: 'Screen-printed SnO<sub>2</sub>/CNT quasi-solid-state gel-electrolyte supercapacitor', *J. Mater. Res. Express*, 2017, **4**, (7), 115501
- [2] Hwang S.W., Hyun S.H.: 'Synthesis and characterization of tin oxide/carbon aerogel composite electrodes for electrochemical supercapacitors', *J. Power Sources*, 2007, **172**, p. 451
- [3] Yan J., Khoo E., Sumboja A., *ET AL.*: 'Facile coating of manganese oxide on tin oxide nanowires with high-performance capacitive behavior', *J. ACS Nano*, 2010, **4**, (7), p. 4247
- [4] Li Z., Chang T., Yun G., *ET AL.*: '2D tin dioxide nanoplatelets decorated graphene with enhanced performance supercapacitor', *J. Alloys Compd.*, 2014, **586**, p. 353
- [5] Bae J., Park Y.J., Yang J.C., *ET AL.*: 'Towards wearable and stretchable fabric-based supercapacitors: novel ZnO and SnO<sub>2</sub> nanowires – carbon fiber and carbon paper hybrid structure', *J. Solid State Electrochem.*, 2015, **19**, p. 211
- [6] Lima S.P., Huang N.M., Lim H.N.: 'Solvothermal synthesis of SnO<sub>2</sub>/graphene nanocomposites for supercapacitor application', *J. Ceramics Int.*, 2003, **39**, p. 6647
- [7] Velmurugana V., Srinivasarao U., Ramachandran R., *ET AL.*: 'Synthesis of tin oxide/graphene (SnO<sub>2</sub>/G) nanocomposite and its electrochemical properties for supercapacitor applications', *J. Mater. Res. Bull.*, 2016, **84**, p. 145
- [8] Kuo S.L., Wu N.L.: 'Composite supercapacitor containing tin oxide and electroplated ruthenium oxide', *J. Electrochem. Solid State Lett.*, 2003, **6**, p. 85
- [9] Kwon O., Deka B.K., Kim J., *ET AL.*: 'Electrochemical performance evaluation of tin oxide nanorod-embedded woven carbon fiber composite supercapacitor', *J. Energy Res.*, 2018, **42**, (2), pp. 490–498, DOI 10.1002/er.3827
- [10] Li R., Ren X., Zhang F., *ET AL.*: 'Synthesis of Fe<sub>3</sub>O<sub>4</sub>@SnO<sub>2</sub> core-shell nanorod film and its application as a thin-film supercapacitor electrode', *J. Chem. Commun.*, 2012, **48**, p. 5010
- [11] Liu C., Yu Z., Neff D., *ET AL.*: 'Graphene-based supercapacitor with an ultrahigh energy density', *J. Nano Lett.*, 2010, **10**, p. 4863
- [12] Selvan R.K., Perelshtein I., Perkash N., *ET AL.*: 'Synthesis of hexagonal-shaped SnO<sub>2</sub> nanocrystals and SnO<sub>2</sub>@C nanocomposites for electrochemical redox supercapacitors', *J. Phys. Chem.*, 2008, **112**, p. 1825
- [13] Li F., Song J., Yang H., *ET AL.*: 'One-step synthesis of graphene/SnO<sub>2</sub> nanocomposites and its application in electrochemical supercapacitors', *J. Nanotechnol.*, 2009, **20**, p. 455602
- [14] Wang W., Hao Q., Lei W., *ET AL.*: 'Graphene/SnO<sub>2</sub>/polypyrrole ternary nanocomposites as supercapacitor electrode materials', *J. RSC Adv.*, 2012, **2**, p. 10268

- [15] Oehl N., Schmuelling G., Knipper M., *ET AL.*: 'In situ X-ray diffraction study on the formation of  $\alpha$ -Sn in nanocrystalline Sn-based electrodes for lithium-ion batteries', *J. CrystEngComm.*, 2015, **17**, p. 8500
- [16] Han Z., Guo N., Li F., *ET AL.*: 'Solvochemical preparation and morphological evolution of stannous oxide powders', *J. Mater. Lett.*, 2001, **48**, p. 99
- [17] Iqbal M.Z., Wang F., Din R.U., *ET AL.*: 'Synthesis of novel clino-pinacoid structure of stannous oxide and hydrogen absorption characteristics', *J. Mater. Lett.*, 2012, **78**, p. 50
- [18] Johari A., Bhatnagar M. C., Rana V.: 'Growth, characterization and I-V characteristics of tin oxide (SnO<sub>2</sub>) nanowires', *J. Adv. Mater. Lett.*, 2012, **3**, p. 515
- [19] Sun S.H., Meng G.W., Zhang G.X., *ET AL.*: 'Raman scattering study of rutile SnO<sub>2</sub> nanobelts synthesized by thermal evaporation of Sn powders', *J. Chem. Phys. Lett.*, 2003, **376**, p. 103
- [20] Xie Y., Zhu F.: 'Electrochemical capacitance performance of polyaniline/tin oxide nanorod array for supercapacitor', *J. Solid State Electrochem.*, 2017, **21**, p. 1675
- [21] Diéguez A., Romano-Rodríguez A., Vilà J A., *ET AL.*: 'The complete Raman spectrum of nanometric SnO<sub>2</sub> particles', *J. Appl. Phys.*, 2001, **90**, p. 1550
- [22] Jang D.M., Jung H., Hoa N.D., *ET AL.*: 'Tin oxide-carbon nanotube composite for NOX sensing', *J. Nanosci. Nanotechnol.*, 2012, **12**, p. 1425
- [23] Cabot A., Arbiol J., Rossinyol Morante E., *ET AL.*: 'Synthesis of tin oxide nanostructures with controlled particle size using mesoporous frameworks', *J. Electrochem. Solid-State Lett.*, 2004, **7**, p. 93
- [24] Tan L., Wang L., Wang Y.: 'Hydrothermal synthesis of SnO<sub>2</sub> nanostructures with different morphologies and their optical properties', *J. Nanomater.*, 2011, **1**, p. 529874
- [25] Marikkannan M., Vishnukanthan V., Vijayshankar A., *ET AL.*: 'A novel synthesis of tin oxide thin films by the sol-gel process for optoelectronic applications', *J. AIP Adv.*, 2015, **5**, p. 027122
- [26] Sinha A.K., Manna P.K., Pradhan M., *ET AL.*: 'Tin oxide with a p-n heterojunction ensures both UV and visible light photo catalytic activity', *J. R. Soc. Chem.*, 2014, **4**, p. 208
- [27] Wang C., Hu Y., Qian Y., *ET AL.*: 'A novel method to prepare nanocrystalline SnO<sub>2</sub>', *J. Nano Structured Mater.*, 1996, **7**, p. 421